Influence of adapting speed on speed and contrast coding in the primary visual cortex of the cat

M. A. Hietanen, N. A. Crowder, N. S. C. Price and M. R. Ibbotson

Visual Sciences, Research School of Biological Sciences, Australian National University, Canberra, ACT 2601, Australia

Adaptation is a ubiquitous property of the visual system. Adaptation often improves the ability to discriminate between stimuli and increases the operating range of the system, but is also associated with a reduced ability to veridically code stimulus attributes. Adaptation to luminance levels, contrast, orientation, direction and spatial frequency has been studied extensively, but knowledge about adaptation to image speed is less well understood. Here we examined how the speed tuning of neurons in cat primary visual cortex was altered after adaptation to speeds that were slow, optimal, or fast relative to each neuron's speed response function. We found that the preferred speed (defined as the speed eliciting the peak firing rate) of the neurons following adaptation was dependent on the speed at which they were adapted. At the population level cells showed decreases in preferred speed following adaptation to speeds at or above the non-adapted speed, but the preferred speed did not change following adaptation to speeds lower than the non-adapted peak. Almost all cells showed response gain control (reductions in absolute firing capacity) following speed adaptation. We also investigated the speed dependence of contrast adaptation and found that most cells showed contrast gain control (rightward shifts of their contrast response functions) and response gain control following adaptation at any speed. We conclude that contrast adaptation may produce the response gain control associated with speed adaptation, but shifts in preferred speed require an additional level of processing beyond contrast adaptation. A simple model is presented that is able to capture most of the findings.

Adaptation is ubiquitous in sensory systems; this is evident both at neural and perceptual levels. For example, in the retina the mechanisms underlying luminance adaptation are well characterized, facilitating the transmission of a broad range of luminance signals despite the limited dynamic range of the retinal circuitry (Rushton, 1965). At a higher level of processing, adaptation to the speed of motion has been characterized psychophysically, with exposure to short periods of motion leading to misrepresentations of absolute speed (Goldstein, 1957; Thompson, 1981) but improvements in speed discriminability (Bex *et al.* 1999; Clifford & Langley, 1999; Clifford & Wenderoth, 1999). However, the purpose and neural locus of this speed adaptation are poorly understood.

There have been several previous neurophysiological investigations that have studied the influence of adaptation on speed tuning using sine-wave gratings. Speed is related to temporal (TF) and spatial frequency (SF) by the equation: speed = TF/SF. Saul & Cynader (1989*a,b*) investigated the influence of adaptation speed on response amplitude in cat primary visual cortex. They showed that

adaptation to moving gratings at a cell's preferred TF and SF generated the largest reductions in response gain. Maddess *et al.* (1988) also recorded from cat primary visual cortex and examined the relationship between various stimulus parameters (including speed and TF) and the adaptation-related reduction in firing rate during the stimulus period. They found that the TF of the stimulus had the most consistent effect on the attenuation of firing rate. In general, response amplitude was reduced maximally when stimulus TFs were high (> 10 Hz). Importantly, when studying speed adaptation it is preferable to use a stimulus that contains many SFs to distinguish true speed adaptation from TF adaptation. In one such study, which used random dot patterns, speed adaptation was shown to cause small shifts in the speed tuning functions of neurons in the middle temporal (MT) area of the monkey cortex (Krekelberg *et al.* 2006*a*). These shifts improved the capacity of neurons to distinguish between different speeds, but the effects were small.

In the present paper, we investigate changes in the speed coding properties of cells in the primary visual cortex of the cat induced by adaptation with aperiodic

gratings (which contain a broad range of SFs), but critically we also investigate the link between speed adaptation and contrast adaptation. Generally, most speed tuning functions are Gaussian-shaped in log-speed space (Fig. 1*A*; also see Priebe *et al.* 2006), while virtually all cells in the primary visual cortices of cats and monkeys produce sigmoidal contrast response functions when response magnitude is plotted as a function of image contrast (Albrecht & Hamilton, 1982). Contrast adaptation has been studied much more extensively than speed adaptation in the primary visual cortex, and both contrast gain control (lateral shifts in the contrast response function following contrast adaptation) and response gain control (compression of the contrast response function following contrast adaptation) have been ascribed functional roles in visual processing (Ohzawa *et al.* 1985; Clifford & Ibbotson, 2002; Wainwright *et al.* 2002; Crowder *et al.* 2006, 2007; Hietanen *et al.* 2007; Durant *et al.* 2007). It is important to examine the interaction between speed and contrast because it is possible that speed adaptation has a distinct functional role in visual processing at the level of primary visual cortex, or it may simply be a manifestation of contrast adaptation in the speed domain.

To investigate the link between contrast and speed adaptation we compared the amount of contrast gain control and measures of speed-related adaptation within single neurons. We were careful to capture both rising and falling phases of each neuron's speed tuning function, thus providing an accurate characterization of the influence of adaptation on the speed tuning of neurons in the visual cortex. Across the population preferred speed did not change following adaptation to speeds below the non-adapted preferred speed of the cells, while adaptation to speeds at or above the non-adapted preferred speed reduced the preferred speed of most cells. Nearly all cells showed an overall reduction in response gain at all test speeds regardless of adaptation speed. Importantly, speed adaptation is not simply an epiphenomenon produced by contrast adaptation because stimuli with the same contrast, but moving at different speeds, can produce radically different changes in speed tuning.

Methods

Physiological preparation

Experimental procedures complied with the guidelines of the Australian National Health and Medical Research Council, and were approved and governed by the Animal Experimentation Ethics Committee of the Australian National University. Data were collected from five adult cats of either sex weighing between 2.8 and 4.2 kg. Animals were initially anaesthetized with ketamine HCl (20 mg kg^{-1}, I.M.) to allow the trachea and right cephalic vein to be cannulated. Depth of ketamine anaesthesia was assessed using the pedal reflex. Anaesthesia during stereotaxic head stabilization and craniotomy was maintained using a mixture of inhaled halothane (1–1.5%) and a 2 : 1 ratio of N_2O and O_2. Neuromuscular blockade was then induced with an intravenous injection of 50 mg of gallamine triethiodide (Flaxedil; Sigma, St Louis, MO, USA) in 2 ml of Hartmann's solution, and maintained with continuous intravenous infusion of Flaxedil at a rate of $10 \text{ mg kg}^{-1} \text{ h}^{-1}$ in a 1 : 1 : 2 mixture of Hartmann's solution, 5% glucose and 8% amino acid solution. Urinary output was confirmed during daily changing of disposable diapers. Expired CO_2 was monitored continuously and maintained at 3.5–4%, and body temperature was maintained at 38°C with an electric heating blanket. Intramuscular injections of Clavulox (1 ml; Pfizer, West Ryde, NSW, Australia), dexamethasone sodium phosphate (1 ml; Ilium, Smithfield, NSW, Australia), and Atropine (0.05 mg kg^{-1}; Apex Laboratories, Somersby NSW, Australia) were administered daily. Corneas were protected with zero-power rigid gas-permeable contact lenses. Pupils were dilated with 1% atropine sulphate eye-drops (Sigma, St Louis, MO, USA), and nictitating membranes were retracted with 0.01% phenylephrine-HCl eye-drops (Sanofi-Synthelabo, NY, USA). Corrective lenses focused the stimulus on the retina at a distance of 57 cm in front of the animal, and 3 mm diameter artificial pupils were placed in front of the eyes. The location of the optic discs was plotted twice daily by reverse ophthalmoscopy. During extracellular recordings the concentration of Halothane was set at 0.5%, but was increased to 1–1.5% whenever we changed electrode tracks or gave injections. Electrocardiogram (ECG) and electroencephalogram (EEG) were monitored continuously. Our policy was that changes in the EEG or ECG that suggested that the level of anaesthesia was not sufficient were managed by increasing the inhaled halothane concentration. Such changes were very rare. Extracellular signals from individual units were acquired with a CED1401 interface and Spike2 software sampled at 40 kHz (Cambridge Electronic Designs, Cambridge, UK).

Stimuli

After isolating a neuron, its dominant eye, receptive field location and spatial structure were qualitatively determined using hand-driven light or dark bars. Only the dominant eye was tested quantitatively, using custom visual stimuli produced by a VSG Series 2/5 stimulus generator (Cambridge Research Systems, Cambridge, UK), and presented on a gamma-corrected monitor (Eizo T662-T, 100 Hz, 57 cd m^{-2} mean luminance, 1024 by 768 pixels) at a viewing distance of 57 cm. Preferred direction, spatial frequency (SF), temporal frequency (TF), and receptive field size and location were calculated using on-line tuning functions. All receptive fields were located

within 10 deg of the area centralis. Neurons in area-17 and -18 were qualitatively classified as simple or complex based on the separability of receptive field regions sensitive to light-on and light-off, as determined using manual stimulation of the receptive field (either light bars on a dark background or dark bars on a light background). Quantitatively, simple and complex cells were classified by calculating the ratio between the first Fourier coefficient (F_1) and mean spiking responses (F_0) to moving sine-wave gratings (Skottun *et al.* 1991; Ibbotson *et al.* 2005; Crowder *et al.* 2006, 2007). Experimental stimuli were presented in a circular aperture the size of the classical receptive field (usually 2–5 deg, with a small number of larger fields in area 18) that was surrounded by a grey of mean luminance (Lum; 57 cd m^{-2}). Sine-wave contrast is defined as:

$$\text{Michelson contrast} = \frac{\text{Lum}_{max} - \text{Lum}_{min}}{\text{Lum}_{max} + \text{Lum}_{min}} \quad (1)$$

Two different experimental stimuli were used. The first was an aperiodic grating, which presented a broad spectrum SF stimulus in order to evaluate speed tuning. The aperiodic grating was generated by convolving a 20 pixel sine-wave from 0 to π radians, with a 1024 pixel seed vector containing values uniformly distributed between 0 and 1. The convolution was performed 3 times, with the resulting vector used to define the luminance of stripes aligned with the cell's preferred orientation (Fig. 1*B*). The convolution operations provide a stimulus with low-pass spatial frequency characteristics with power in the band ranging from 0.05 cpd to 1 cpd (Fig. 1*B*). The spatial frequency content of these aperiodic stimuli is known to cover the sensitivity range of most cells in areas-17 and -18 (Movshon *et al.* 1978; Casanova *et al.* 1995). The stimulus had a root mean square (RMS) contrast of 0.15. The stripes of this aperiodic grating were aligned with the cell's preferred orientation, and moved in the cell's preferred direction. Test speeds were presented in random order for 12 repetitions. Non-adapted speed tuning was determined by presenting an aperiodic grating moving at 10 speeds (either 1–60, 1–128, or 1–196 deg s^{-1} depending on the cell being tested) for 1 s followed by 4 s of mean luminance. In each adaptation condition the same test speeds were presented, but the first test was preceded by 60 s of motion at the adaptation speed, and each test was followed by a period of 4 s of motion at the adaptation speed. Each cell was adapted to three speeds derived from the non-adapted speed tuning function: (1) adaptation at the peak speed (V_{100}); (2) the speed that elicited 50% of the non-adapted maximum response that was slower than the optimum speed (VL_{50}); and (3) the speed that elicited 50% of the non-adapted maximum response that was faster than the optimum speed (VH_{50}). These three speeds are shown as vertical arrows in Fig. 1. Each adaptation run was followed by a 3–5min gap to allow the cell to recover

from the adaptation. Furthermore, adaptation tests were followed by a repeat of the non-adapted control.

The second stimulus was an optimally orientated sine-wave grating used to generate contrast response functions at the cell's VH_{50} and VL_{50}. For this stimulus, the SF was set to the cell's optimum as determined from preliminary testing, and the TF was adjusted to produce speeds equal to the cell's VL_{50} and VH_{50} (speed = TF/SF). High (VH_{50}) and low (VL_{50}) speed contrast response functions were generated by presenting moving sine-wave
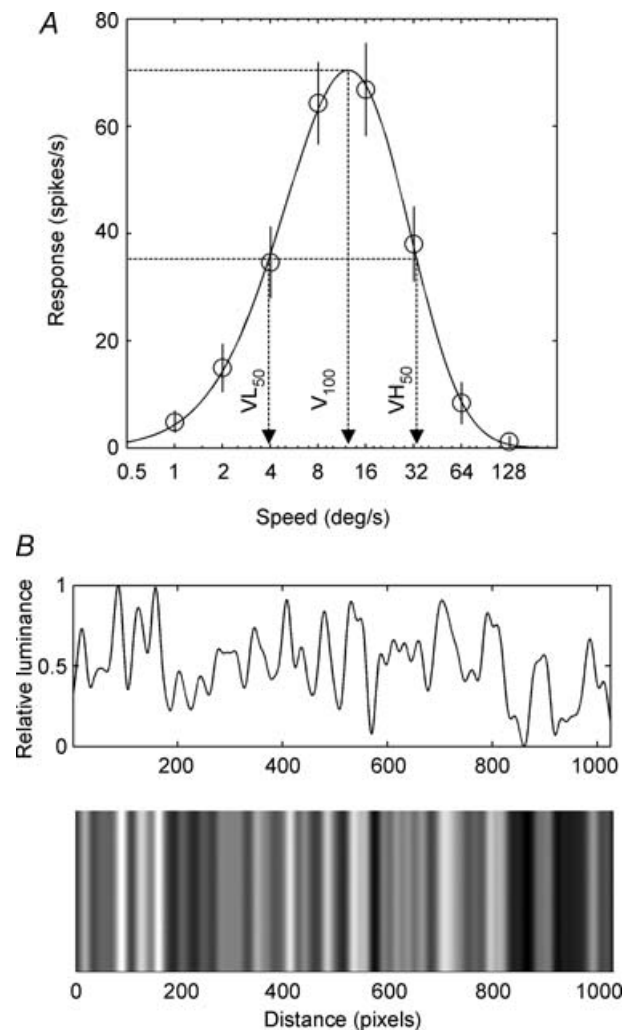

Figure 1. Response of an area-17 neuron to aperiodic gratings moving at different speeds
A, an example speed tuning response function from an area-17 neuron. Mean spiking responses (ordinate) to various test speeds (abscissa) were fitted to a skewed Gaussian function (continuous line; see Methods). The arrows show the peak of the function and the two semisaturation points. For each cell, these three speeds were used as the adapting speeds: the preferred speed (V_{100}); the slower speed that elicited 50% of the non-adapted max response (VL_{50}); and the faster speed that elicited 50% of the non-adapted max response (VH_{50}). Error-bars are ± 1 s.e.m. *B*, a schematic diagram of the aperiodic grating used in the experiment with the luminance waveform shown above the example stimulus.

gratings at 11 different contrasts (0.04–1) for 0.5 s tests interleaved with 4 s of mean luminance. Adapted contrast response functions were collected at both VH_{50} and VL_{50} by presenting 60 s of initial adaptation to a contrast of 0.32 followed by 0.5 s tests (aforementioned test contrasts) and 4 s top ups (contrast = 0.32).

Quantitative analysis

Neuronal responses to individual stimulus repetitions were aligned relative to a synchronization pulse provided by the stimulus generation computer in the blanking interval prior to the first stimulus frame. Responses are represented as spike density functions (SDFs) with bin-widths of 1 ms generated by initially convolving a delta function at each spike arrival time with a Gaussian window ($\sigma = 3$ ms). SDFs were then calculated by averaging responses to individual stimulus presentations.

Response-shift. Response-shift is a relative measure of how much the response rate (in spikes s^{-1}) was changed by adaptation. In all cases where a response-shift statistic was calculated the following formula was used:

$$\text{Response-shift}(ij) = \frac{R_{\max(ij)} - R_{\max(0j)}}{R_{\max(ij)} + R_{\max(0j)}} \quad (2)$$

where Response-shift(ij) is the response-shift when adapted at speed i and tested at speed j, $R_{\max(ij)}$ is the maximum response of the cell when tested at speed j, after adaptation at speed i, and $R_{\max(0j)}$ is the non-adapted maximum response of the cell when tested at speed j. This statistic ranges from -1 to 1. Negative values indicate that the $R_{\max}$ following adaptation was smaller than the non-adapted $R_{\max}$. Positive values indicate that the adapted $R_{\max}$ was greater than the non-adapted $R_{\max}$.

Speed. The responses to stimulation at various speeds were calculated by averaging the firing rate from 100 ms after motion onset to the end of motion (1000 ms). The first 100 ms of the response was not counted as it contained a large onset transient that was critically dependent on the first few time-locked spikes. Inclusion of the onset transient did not influence the overall properties, as outlined here, but did tend to push the mean firing rates at all tested speeds to higher values. As this increase in apparent firing rate was due to the time-locked onset transient and not to a specific speed-related effect, we discounted the onset transient from the data. The responses to speed were fitted with a skewed-Gaussian function and then had the spontaneous firing rate subtracted from them:

$$R_x = R_{\max} \exp\left(-\left(\frac{\log(x/x_{\text{peak}})}{B + A\log(x/x_{\text{peak}})}\right)^2\right) + R_{\text{Spont}} \quad (3)$$

where R_x is the response at speed x; $R_{\max}$ controls the amplitude; x_{peak} is the cell's peak speed, at which the peak spiking rate $R_{\max}$ occurs; A controls the skew of the curve; and B is the bandwidth. R_{Spont} is the measured spontaneous activity and was not allowed to vary as part of the least-squares fitting routine. Goodness of fit to the curve was measured with r^2 values, and across all fits this measure formed a highly skewed distribution with a median of 0.90 and 25th and 75th percentiles of 0.83 and 0.95, respectively.

Speed-shift statistics were calculated using:

$$\text{Speed-shift}(ij) = \frac{x_{\text{peak}(ij)} - x_{\text{peak}(0j)}}{x_{\text{peak}(ij)} + x_{\text{peak}(0j)}} \quad (4)$$

where, Speed-shift(ij) is the speed-shift when adapted at speed i and tested at speed j, $x_{\text{peak}(ij)}$ is the peak speed of the cell when tested at speed j, after adaptation at speed i, and $x_{\text{peak}(0j)}$ is the non-adapted peak speed of the cell when tested at speed j. This statistic ranges from -1 to 1. Negative values indicate that the peak speed following adaptation was slower than the non-adapted peak speed. Positive values indicate that the adapted peak speed was faster than the non-adapted peak speed.

Contrast. The neuronal responses to contrast were fitted with a sigmoid function after subtracting the spontaneous firing rate:

$$R(ci) = \frac{R_{\max} \times c^n}{c^n + C_{50}^n} + M \quad (5)$$

where $R(ci)$ is the amplitude of the evoked response at contrast ci, M is the spontaneous rate, n is the exponent that determines the steepness of the curve, $R_{\max}$ is the maximum elevation in response above the spontaneous rate, and C_{50} is the contrast that generates a response elevation of half $R_{\max}$. Goodness of fit to the curve was measured with r^2 values, and across all fits this measure formed a highly skewed distribution with a median of 0.96 with 25th and 75th percentiles of 0.91 and 0.98, respectively. Rarely, contrast response functions did not show saturation at higher contrasts; in these cases the upper and lower $R_{\max}$ bounds for the fit were set at $\pm 10\%$ of the maximum measured neuronal response above spontaneous.

Contrast-shift was calculated as:

$$\text{Contrast-shift}(ij) = \frac{C_{50(ij)} - C_{50(0j)}}{C_{50(ij)} + C_{50(0j)}} \quad (6)$$

where, Contrast-shift(ij) is the contrast-shift when adapted at speed i and tested at speed j, $C_{50(ij)}$ is the C_{50} of the cell when tested at speed j, after adaptation at speed i, and $C_{50(0j)}$ is the non-adapted C_{50} of the cell when tested at speed j. Once again, this statistic ranges from -1 to 1, with negative values indicating that the C_{50} following adaptation was at a lower contrast than the non-adapted C_{50}. Positive values indicate that the adapted C_{50} was at a higher contrast than the non-adapted C_{50}.

Direction index. The directionality of cells was tested using the following equation:

$$\text{Direction index} = \frac{[\text{spikes/s}_{\text{preferred}} - \text{spikes/s}_{\text{anti-preferred}}]}{[\text{spikes/s}_{\text{preferred}} + \text{spikes/s}_{\text{anti-preferred}}]} \tag{7}$$

A value close to 1 indicates a highly direction-selective cell, while a value close to zero indicates a non-directional cell.

Histology

At the conclusion of recording sessions, animals were given a lethal dose of pentobarbitone sodium (120–180 mg depending on animal's weight) and quickly perfused with ice cold saline (0.9%) followed by 10% formol saline. Brains were sectioned and electrode tracks were reconstructed using established procedures (Crowder *et al.* 2006; Price *et al.* 2006). The electrode tracks we used moved parallel to the cortical layers on the medial bank of the marginal sulcus (penetration angle outlined in Crowder *et al.* 2006). We aimed to obtain cells from area-17, but histological reconstructions revealed that 13 out of 97 cells (at the bottom of the electrode tracks) were in area-18.

Results

We recorded from 117 neurons; of these 20 neurons were excluded due to poor fits ($r^2 < 0.3$) to either their contrast or speed tuning functions. Of the 97 neurons that remained, 86 were in area-17 (8 simple and 76 complex) and 13 in area-18 (4 simple and 9 complex). Clearly, our study was heavily biased towards complex cells from area-17 (78% of cells). However, we have left the other neurons in the analysis for comparative purposes. The speed tuning characteristics of simple and complex cells (in both areas) were compared using Kruskal–Wallis ANOVA. The only significant difference between cell types was that area-18 cells preferred higher speeds (median = 40.5 deg s^{-1}) than area-17 cells (median = 17.8 deg s^{-1}), $P < 0.01$. This finding accords with previous studies (Movshon *et al.* 1978). Using a direction index (DI; eqn (7)), we found that 71/97 cells had DI < 0.6. The remaining 27% of cells were strongly directional (DI > 0.6). There were no significant differences in the non-adapted speed tuning functions or post-adaptation changes when cells with a DI greater than 0.6 were compared to cells with a DI < 0.6 (Kruskal–Wallis ANOVA, $P > 0.1$).

We measured the speed tuning functions of neurons using an aperiodic grating stimulus. The three columns in Fig. 2 show the non-adapted (continuous line) and adapted (dashed line) speed tuning of three representative neurons in response to adaptation at the cells' VL$_{50}$ (top row), V_{100} (middle row), and VH$_{50}$ (bottom row). In virtually all cells the overall amplitude of the speed tuning function was reduced following adaptation regardless of the speed at which adaptation occurred. This phenomenon is referred to as response gain control. In most cells, the preferred speed also changed following adaptation. The cell in Fig. 2*A–C* shows repulsive shifts in speed following adaptation. In this case, adaptation at speeds below the non-adapted peak increase preferred speed (Fig. 2*A*), and adaptation at speeds above the non-adapted peak decrease preferred speed (Fig. 2*C*). Figure 2*D–F* shows an example cell that shifts its preferred speed toward slow speeds regardless of adaptation speed. Finally, Fig. 2*G–I* presents a cell that increased its preferred speed following adaptation at any speed. Cells that did not shift their preferred speeds following speed adaptation (not shown) still exhibited strong response gain control. The adaptation behaviours that were qualitatively described above appeared to form a continuum across the cell population. At the extreme ends of the continuum were cells that increased or decreased their preferred speeds irrespective of the adapting speed, and in the middle of the continuum were cells that showed repulsive shifts in preferred speed or did not change their preferred speeds following adaptation. While some of the example cells shown in Fig. 2 appear to have a reduced bandwidth following adaptation, this decrease was not consistently different from zero at the population level (*t* tests, $P > 0.1$).

To quantify the shifts in preferred speed that are associated with adaptation we calculated the speed-shift (eqn (4)). Negative values of speed-shift indicate a reduced preferred speed, while positive values indicate an increased preferred speed. Similarly, changes in maximum response following adaptation for each cell were normalized using a response-shift statistic (eqn (2)). Figure 3 shows the speed-shift (Fig. 3*A,C* and *E*) and response shift (Fig. 3*B, D* and *F*) values for the population of cells. At the population level there was no systematic speed-shift following adaptation at VL$_{50}$ (Fig. 3*A*; $X = -0.009$, s.d. $= 0.239$), but significantly negative speed shifts following adaptation to V_{100} (Fig. 3*C*; $X = -0.135$, s.d. $= 0.278$) and VH$_{50}$ (Fig. 3*E*; $X = -0.157$, s.d. $= 0.202$) (*t* tests, $P < 0.01$). Cells that decreased their preferred speed following adaptation at any speed and cells that showed repulsive speed shifts were more common than cells that always

increased their preferred speed following adaptation, and this is reflected in the population data by the abundance of negative speed shift values for V_{100} and VH_{50} but a VL_{50} distribution centred around zero.

Cells' spike rates were lower following adaptation, as evidenced by significantly negative response shifts regardless of adaptation speed (t tests, $P < 0.01$). This negative response shift was generally greatest following adaptation at V_{100} (Fig. 3D; $X = -0.350$, s.d. $= 0.225$). Adaptation at VL_{50} produced a moderate negative response shift (Fig. 3B; $X = -0.290$, s.d. $= 0.264$) and adaptation at VH_{50} produced a smaller negative response shift (Fig. 3F; $X = -0.185$, s.d. $= 0.285$). The speed and response shifts were not correlated following adaptation at VL_{50}

($r = -0.058$, $P > 0.1$), V_{100} ($r = 0.120$, $P > 0.1$) and VH_{50} ($r = 0.085$, $P > 0.1$).

Relationship with contrast adaptation

In the previous section we used an aperiodic grating to measure speed coding. It is difficult to use this stimulus to measure contrast coding because the contrast in each patch of the stimulus as it passes through a cell's receptive field is not consistent. Therefore, we used sinusoidal gratings to measure contrast response functions from 49/97 cells. The contrast response functions were measured at speeds that equated to VL_{50} and VH_{50} (see methods), and fitted with sigmoidal functions to extract C_{50} and R_{max} values.
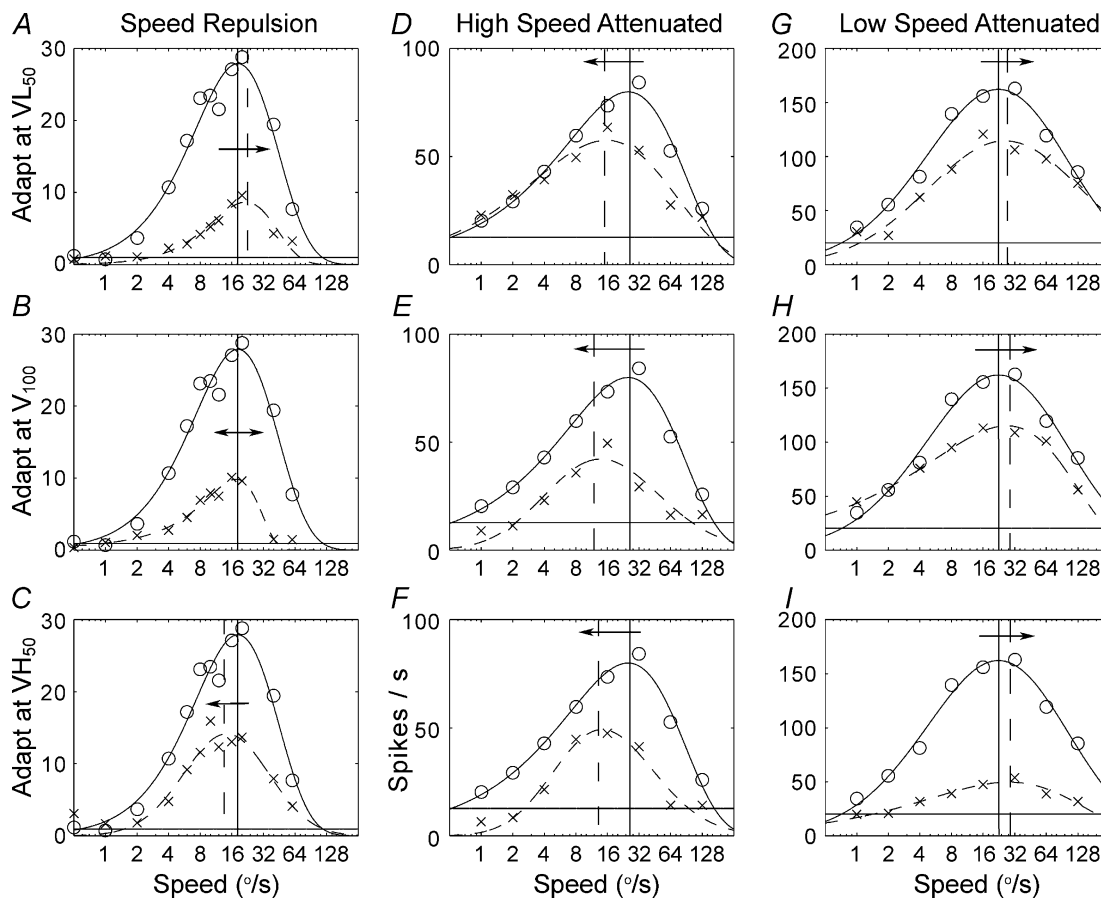

Figure 2. Speed tuning of three example neurons (columns) before and after adaptation to low (top row), peak (middle row), and high speeds (bottom row)
For all graphs speed (abscissa) is plotted against spikes per second (ordinate). Circles and continuous lines represent mean responses and skewed-Gaussian fits in the non-adapted case, respectively. × and dashed lines represent mean responses and skewed-Gaussian fits in the adapted case, respectively. The cell shown in *A–C* displays speed repulsion following adaptation to low (*A*), peak (*B*) and high speeds (*C*). This cell increases its preferred speed following low speed adaptation and decreases it following high speed adaptation. The preferred speed remains unchanged following adaptation at the peak speed. The cell shown in *D–F* decreases its preferred speed following adaptation at any speed. The cell shown in *G–I* increases its preferred speed following adaptation at any speed. Filled and dashed vertical lines represent non-adapted and adapted peak speeds, respectively. Arrows indicate whether peak speed is increasing (rightward arrows), decreasing (leftward arrows), or unchanged (double-headed arrows).

Figure 4 shows example contrast response functions from a typical cell prior to adaptation (open circles) and then following adaptation (filled circles) at VL_{50} (Fig. 4*A*) and VH_{50} (Fig. 4*B*). The error bars in Fig. 4 are ± 1 s.e.m. During these experiments, we attempted to keep the maximum firing rate (R_{max}) at similar levels during stimulation by using speeds that induced similar responses (VL_{50} and VH_{50}), thus limiting the potential effect of spiking rate on adaptation. However, subsequent analyses revealed that testing at VH_{50} tended to elicit spiking rates slightly higher than testing at VL_{50} ($X = 14.85$ spikes s^{-1}, s.d. $= 38.03$, t test $P < 0.05$). There were significant differences between the C_{50} values at low (mean $= 0.37$) and high (mean $= 0.47$) speeds (t test, $P < 0.05$).

After the control values were collected, cells were adapted and tested at VL_{50} and then adapted and tested

at VH_{50}. C_{50} and R_{max} values were used to generate response-shift (eqn (2)) and contrast-shift (eqn (6)) statistics for the contrast domain, respectively. Figure 5 plots the speed-shift values from the speed adaptation protocol against contrast-shift values from the contrast adaptation protocol for VL_{50} (Fig. 5*A*) and VH_{50} (Fig. 5*B*). When adapted at their VL_{50} values 34 (69%) cells showed contrast gain control (positive contrast-shift; Fig. 5*A*) and the contrast and speed shifts were weakly correlated ($r = -0.25$, $P < 0.1$). When adapted at their VH_{50} values, all but nine cells showed positive contrast-shifts (Fig. 5*B*) and there was no correlation between the two shift statistics ($r = -0.04$, $P = 0.76$). Figure 6 shows the response-gain statistic measured using the contrast adaptation protocol (abscissa) and the speed adaptation protocol (ordinate) following adaptation at VL_{50} (Fig. 6*A*) and VH_{50} (Fig. 6*B*). For both speed conditions, the majority of points are located in the lower left quadrant. It is clear that reductions in response gain occur for both speed and contrast protocols, and for all adaptation speeds. Furthermore, the response shifts collected using speed adaptation and those
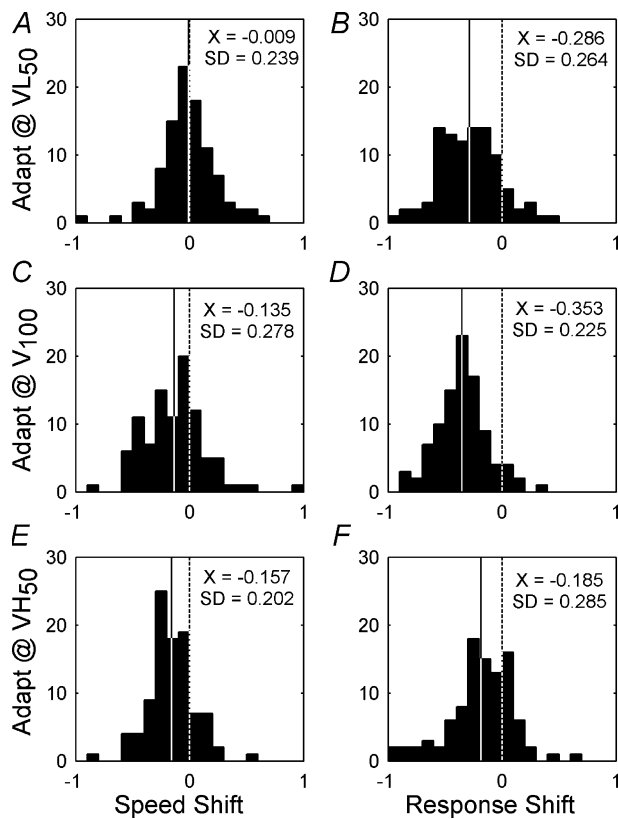

Figure 3. Histograms showing the response and speed shifts across the population following adaptation at VL_{50}, V_{100} and VH_{50} speeds
Dashed vertical lines indicate no change. Continuous vertical lines indicate the population mean ($X \pm$ s.d.). For the speed shift statistic, negative values indicate reductions in preferred speed following adaptation while positive values indicate increases. Following adaptation at VL_{50} (*A*) there is on average no change in the preferred speed of the neurons. Following adaptation at V_{100} (*C*) and VH_{50} (*E*) there is a significant decrease in the preferred speed of the cells. For the response shift statistic (*B*, *D* and *F*) the maximum responses of the neurons, on average, are reduced following adaptation at any speed.
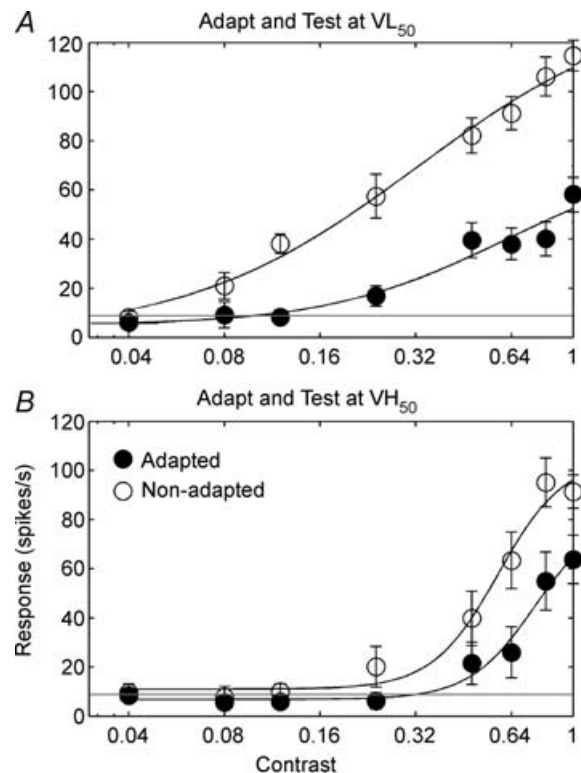

Figure 4. Changes in the contrast response functions of an example cell following adaptation to VL_{50} (*A*) and VH_{50} (*B*)
For both graphs contrast (abscissa) is plotted against spikes per second (ordinate). Open circles represent the non-adapted case while the filled circles represent the adapted case. Continuous lines show the best fit to a sigmoid (see Methods). Dashed horizontal lines represent the spontaneous firing rate. Response gain can be seen as a reduction of the maximum firing rate while contrast gain is a shift in the contrast response function along the log-contrast axis toward higher contrasts.

collected using contrast adaptation are correlated at VL_{50} ($r = 0.31$, $P < 0.03$) and VH_{50} ($r = -0.34$, $P < 0.02$).

Discussion

We measured the speed tuning functions of area-17 and -18 cells following adaptation at the speed eliciting the peak response for each neuron (V_{100}) as well as the speeds eliciting half-maximal responses (rising edge: VL_{50} and falling edge: VH_{50}). Our results show that most cells in the primary visual cortex undergo clear and consistent changes

in their speed tuning functions following adaptation. These differences consist of both a reduction in the absolute responsiveness of the cells and differential changes in the speed that elicits the maximum response of the cell based on the history of prior stimulation (Fig. 3). Specifically, cells tended to reduce their preferred speed following adaptation at or above the non-adapted preferred speed of the cell. When adapted at a speed below
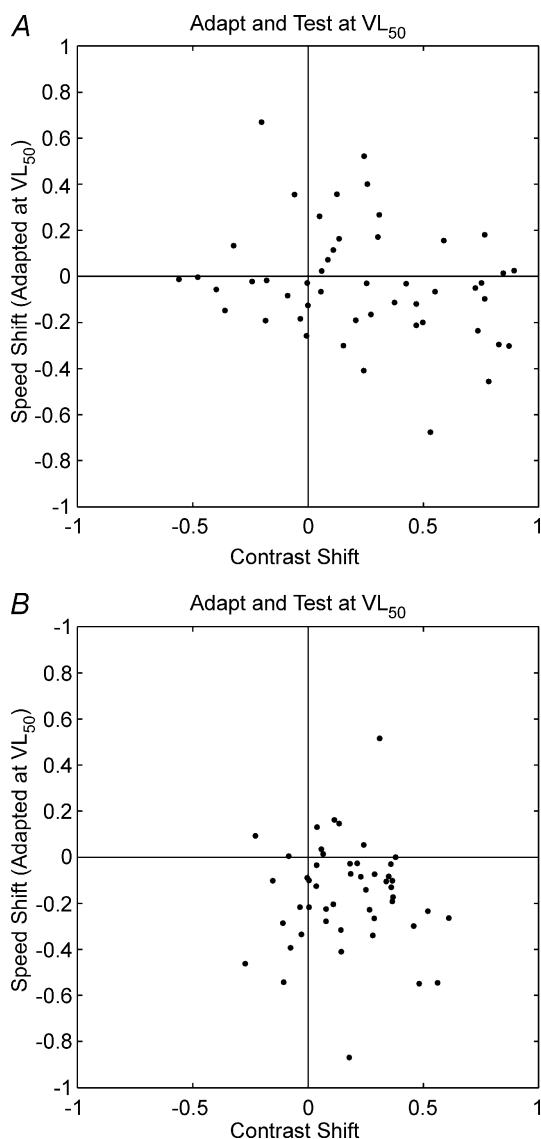

Figure 5. Relationship between contrast gain control and shifts in preferred speed following adaptation
Scatter plots showing speed-shift (ordinate) as a function of contrast-shift (abscissa) following low (*A*) and high (*B*) speed adaptation for each cell. Points to the right of the vertical line indicate an increase in C_{50} following adaptation (contrast gain control). Points below the horizontal line indicate a reduction in the peak speed of the cell following adaptation.
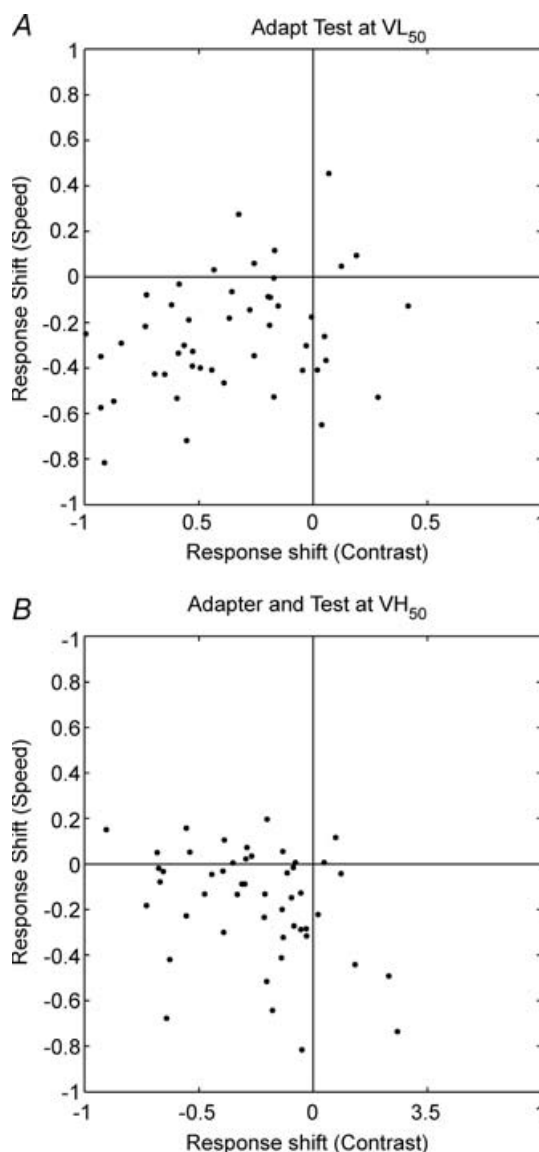

Figure 6. Response gain control elicited by contrast and speed adaptation
Scatter plots showing response-shift induced by speed adaptation (ordinate) as a function of response-shift induced by contrast adaptation (abscissa) following low (*A*) and high (*B*) speed adaptation. Points to the left of the vertical line and below the horizontal line show a decrease in maximum firing rate following adaptation (response gain). Response gain is present in almost all cells following adaptation at either speed when using either the contrast tuning protocol or the speed tuning protocol.

the non-adapted preferred speed they did not shift their preferred speed subsequent to adaptation.

Previous studies using psychophysical methodology to examine the perceptual consequences of speed adaptation have shown that perceived speed is reduced (Goldstein, 1957; Thompson, 1981; Krekelberg *et al.* 2006*a*) and that speed discriminability (the ability to discriminate two simultaneously or sequentially presented speeds) is improved following speed adaptation (Clifford & Langley, 1996; Bex *et al.* 1999; Clifford & Wenderoth, 1999; Krekelberg, van Wezel & Albright, 2006*a*). These perceptual studies of speed adaptation have typically used speeds of less than $24 \deg s^{-1}$ while in our study often the adaptation speeds were typically higher than this (particularly at V_{100} and VH_{50}). If the bandwidth of the speed tuning functions had become narrower following adaptation it could have conceivably produced enhanced discriminability. Our data showed no significant difference in the bandwidth of the cells when the non-adapted speed tuning functions were compared to those obtained following adaptation. It is important to note that for any rate-coded representation of a stimulus the per-cell accuracy will be reduced where the firing rate change is low for a given change in speed. For the Gaussian speed tuning curves this occurs at the peak of the tuning function. By changing the speed that elicits the peak firing away from the non-adapted preferred speed a cell relying on a spiking-rate code will improve its accuracy around the non-adapted preferred speed.

We also measured non-adapted and adapted contrast response functions from 49 cells in this study. Nearly all of these cells showed contrast gain and response gain control irrespective of the type of speed adaptation observed and the response gain obtained following speed adaptation was correlated with that obtained using contrast adaptation. However, stimuli with the same contrast, but moving at different speeds, produced radically different changes in speed and contrast tuning. For example, some cells showed repulsive changes in peak speed following adaptation such that low speed adaptation shifted the preferred speed higher and high speed adaptation shifted the cell's preferred speed to lower values (Fig. 2*A–C*). We therefore conclude that while the response gain observed in speed adaptation may be produced by contrast adaptation, adaptation to contrast alone cannot explain shifts in preferred speed elicited by speed adaptation. Psychophysical observations have suggested that while contrast and speed adaptation often co-occur, reductions in perceived speed are not dependent on reductions in perceived contrast (Bex *et al.* 1999). Our data support the view that speed adaptation requires additional mechanisms beyond contrast adaptation and is therefore in line with psychophysical observations. The perception of speed has been linked with area MT in the macaque (Liu & Newsome, 2005), and cells in MT show changes in

speed coding after adaptation (Krekelberg *et al.* 2006*a,b*). However, it is not known how these changes are related to contrast adaptation.

A simple model of speed adaptation in early visual cortex

The simplest model that can explain the continuum of shifts in preferred speed following adaptation is if the tuning function of an individual cell in the primary visual cortex is derived from two overlapping speed tuned channels. In this two-channel model, the input speed channels undergo activity-dependent response gain, and the different speed adaptation changes are created by adjusting the susceptibility of each speed channel to response gain (some input channels adapt while others do not). Figure 7 shows the speed tuning of a hypothetical
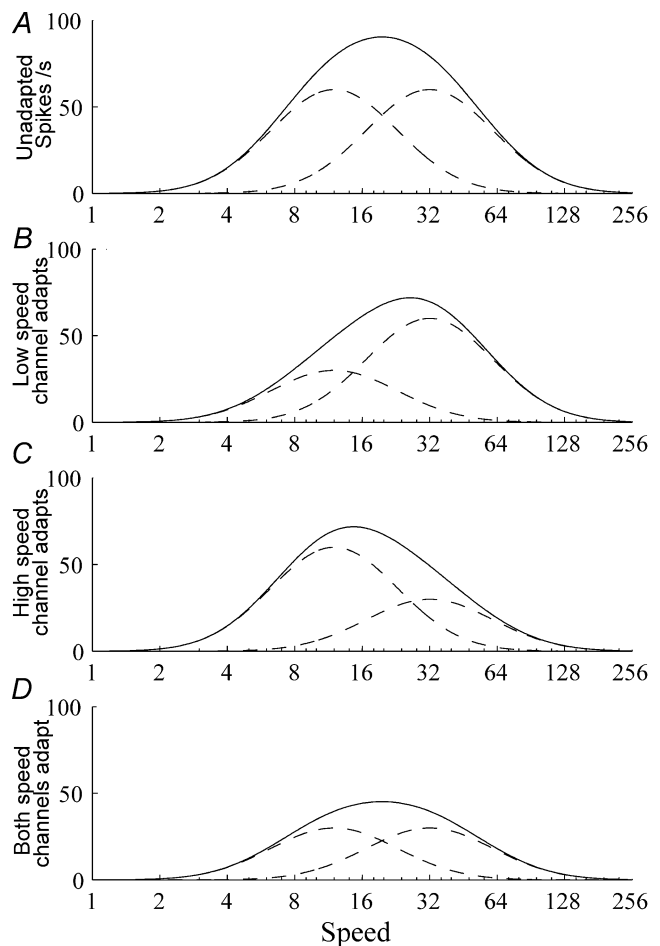

Figure 7. Two-channel model of speed adaptation
A shows the speed tuning of a hypothetical cell (continuous line) created by adding the inputs of two separately speed tuned inputs (dashed lines). Adapting the low speed input will reduce its response and skew the tuning curve away from it toward higher speeds (*B*). Adaptation that reduces the high speed input skews the tuning curve to lower speeds (*C*). Adaptation at the peak speed reduces both inputs equally, and decreases the amplitude of the tuning curve without changing the location of its peak (*D*).

cell (continuous line), that receives inputs from two speed-tuned channels (dashed lines). For cells that respond in a manner consistent with speed repulsion (Fig. 2A–C), both input channels are susceptible to response gain reduction. Adaptation at a low speed (VL$_{50}$) produces a reduction in the response gain of the low-speed channel, thus shifting the preferred tuning of the overall system to higher speeds (Fig. 7B), and adaptation at VH$_{50}$ causes the reverse effect (Fig. 7C). Adaptation at the preferred speed causes a reduction in the gain of both channels and therefore a reduction in overall gain (Fig. 7D). As the gain of both input channels is reduced equally, the preferred speed remains constant (Figs 7D and 3B). If only the high speed channel is susceptible (or relatively more susceptible) to response gain, the preferred speed would decrease following adaptation to any speed (as shown in Fig. 2D–F). Likewise, if only the low speed channel is susceptible to response gain, the preferred speed would increase following adaptation to any speed (see the neuron in Fig. 2G–I). Cells that do not shift preferred speed following adaptation (not shown) could be conceptualized as cells receiving input from a single speed channel. It is noteworthy that these cells exhibit contrast gain control exclusively.

An important limitation of our two-channel model is that it assumes that adaptation is firing rate dependent. In this model, the speed tuning of a single input channel is fixed, and it will only adapt to speeds that are within its response bandwidth. This activity-dependent adaptation could realistically be implemented using a number of ionic conductances (e.g. Na$^+$- or Ca^{2+}-activated K$^+$ currents; Schwindt *et al.* 1988, 1989, 1992; Pennefather *et al.* 1985; Foehring *et al.* 1989; Sah, 1996). For example, Sanchez-Vives *et al.* (2000b) demonstrated that the slow K$^+$ current that generates the hyperpolarization to mediate spike frequency adaptation in slices of ferret primary visual cortex was dependent on the presence of Na$^+$ or Ca^{2+}. However, it has been shown to be the case for contrast adaptation in the primary visual cortex at least, that adaptation does not depend entirely on firing rate (Vidaysagar, 1990; Crowder *et al.* 2006). A more thorough understanding of the cellular mechanisms and circuits underlying various forms of adaptation will no doubt pave the way for more realistic and comprehensive models of speed and contrast tuning.

Thalamic influences on cortical speed adaptation

If the differential speed adaptation effects in our sample population are the result of selective adaptation of 'speed channels' projecting to area-17 and -18 neurons, the obvious candidates for these inputs are cells in the dorsal lateral geniculate nucleus (dLGN). The dLGN is the origin of two major feed-forward pathways to the primary visual cortex: X- and Y-type cells. X- and Y-type cells provide inputs to area-17 and -18, respectively, but there is significant cross-talk between the two areas (for reviews see Stone & Dreher, 1973; Dreher *et al.* 1980; Burke *et al.* 1992; Dreher *et al.* 1992). The two pathways have different mean speed preferences with Y-cells preferring higher speeds than X-cells. Orban *et al.* (1985) showed for bar stimuli that cat X-cells are tuned most often to speeds of 10–100 deg s^{-1}, while Y-cells are tuned most often for speeds of 70–500 deg s^{-1}. It is unclear how speed selectivity might be altered by the neural transformations that produce orientation and direction selectivity in primary visual cortex from centre–surround dLGN inputs. However, it is worth noting that peak speeds of cells within our population lie within the range of X-cells. Many of the cortical cells in our sample still responded strongly out to speeds of 256 deg s^{-1}, allowing for the possibility of some Y-cell inputs as well.

Is it plausible that the speed-dependent response gain control of the two input channels in our model arises from contrast adaptation in dLGN? Until recently, it was believed that cells in the dLGN did not show contrast adaptation (e.g. Maffei *et al.* 1973; Movshon & Lennie, 1979; Derrington *et al.* 1984; Ohzawa *et al.* 1985). However, several groups have been able to demonstrate contrast adaptation in cat and monkey dLGN. In cats, 46% of X- and Y-type cells in the dLGN showed some form of contrast adaptation, although only 18% of cells showed contrast gain control (Shou *et al.* 1996). Sanchez-Vives *et al.* (2000a) also noted consistent but modest contrast adaptation in cat dLGN. Strong adaptation has been observed in magnocellular cells of the monkey LGN for high drift-rates (usually tested at 11 Hz), but preliminary reports suggest that high drift rates do not induce adaptation in cat thalamus (communicated via Carandini, in Solomon *et al.* 2004).

The various contrast adaptation effects observed in dLGN by different authors produce different predictions for the two-channel model. The findings of Shou *et al.* (1996) that about half of the dLGN neurons adapt while the rest do not is consistent with our model. As described above, the various combinations of adapting and non-adapting speed channels could explain all of our speed adaptation categories. The findings of Sanchez-Vives *et al.* (2000a) predict only the general decrease in response gain that was observed in our population. Finally, if neurons in the cat dLGN showed robust adaptation to high speeds as shown in the monkey (Solomon *et al.* 2004), a preponderance of cells displaying high speed attenuation (Fig. 2D–F) would be expected.

References

Albrecht DG & Hamilton DB (1982). Striate cortex neurons in monkey and cat: contrast response function. *J Neurophysiol* **48**, 217–237.

Bex PJ, Bedingham S & Hammett ST (1999). Apparent speed and speed sensitivity during adaptation to motion. *J Opt Soc Am A* **16**, 2817–2824.

Burke W, Dreher B, Michalski A, Cleland BG & Rowe MH (1992). Effects of selective pressure block of Y-type optic nerve fibers on the receptive-field properties of neurons in the striate cortex of the cat. *Vis Neurosci* **9**, 47–64.

Casanova C, Savard T, Nordmann JP, Molotchnikoff S & Minville K (1995). Comparison of the responses to moving texture patterns of simple and complex cells in the cats area-17. *J Neurophysiol* **74**, 1271–1286.

Clifford CWG & Ibbotson MR (2002). Fundamental mechanisms of visual motion detection: models, cells and functions. *Prog Neurobiol* **68**, 409–437.

Clifford CWG & Langley K (1996). Psychophysics of motion adaptation parallels insect electrophysiology. *Curr Biol* **6**, 1340–1342.

Clifford CWG & Langley K (1999). Adaptation to temporal modulation can enhance differential speed sensitivity. *Vis Res* **39**, 4324–4332.

Clifford CWG & Wenderoth P (1999). Adaptation to temporal modulation can enhance differential speed sensitivity. *Vis Res* **39**, 4324–4332.

Crowder NA, Price NS, Hietanen MA, Dreher B, Clifford CW & Ibbotson MR (2006). Relationship between contrast adaptation and orientation tuning in V1 and V2 of cat visual cortex. *J Neurophysiol* **95**, 271–283.

Crowder NA, Van Kleef J, Dreher B & Ibbotson MR (2007). Complex cells increase their phase sensitivity at low contrasts and following adaptation. *J Neurophysiol* **98**, 1155–1166.

Derrington AM, Krauskopf K & Lennie P (1984). Chromatic mechanisms in lateral geniculate nucleus of macaque. *J Physiol* **357**, 241–265.

Dreher B, Leventhal AG & Hale PT (1980). Geniculate input to cat visual cortex: a comparison of area 19 with areas 17 and 18. *J Neurophysiol* **44**, 804–826.

Dreher B, Michalski A, Cleland BG & Burke W (1992). Effects of selective pressure block of Y-type optic nerve fibers on the receptive-field properties of neurons in area 18 of the visual cortex of the cat. *Vis Neurosci* **9**, 65–78.

Durant S, Clifford CWG, Crowder NA, Price NSC & Ibbotson MR (2007). Informational basis of cortical contrast adaptation. *J Opt Soc Am A* **24**, 1529–1537.

Foehring RC, Schwindt PC & Crill WE (1989). Norepinephrine selectively reduces slow Ca^{2+}- and Na^+ mediated K^+ currents in cat neocortical neurons. *J Neurophysiol* **61**, 245–256.

Hietanen MA, Crowder NC & Ibbotson MR (2007). Contrast gain control is drift-rate dependent: An informational analysis. *J Neurophysiol* **97**, 1078–1087.

Ibbotson MR, Price NSC & Crowder NA (2005). On the division of cortical cells into simple and complex types: a comparative viewpoint. *J Neurophysiol* **93**, 3699–3702.

Krekelberg B, van Wezel RJ & Albright TD (2006a). Adaptation in macaque MT reduces perceived speed and improves speed sensitivity. *J Neurophysiol* **95**, 255–270.

Krekelberg B, van Wezel RJ & Albright TD (2006b). Interactions between speed and contrast tuning in the middle temporal area: Implications for the neural code for speed. *J Neurosci* **26**, 8988–8998.

Liu J & Newsome WT (2005). Correlation between speed perception and neural activity in the middle temporal visual area. *J Neurosci* **25**, 711–722.

Maddess T, McCourt ME, Blakeslee B & Cunningham RB (1988). Factors governing the adaptation of cells in area-17 of the cat visual cortex. *Biol Cybern* **59**, 229–236.

Maffei L, Fiorentini A & Bisti S (1973). Neural correlate of perceptual adaptation to gratings. *Science* **182**, 1036–1038.

Movshon JA & Lennie P (1979). Pattern-selective adaptation in visual cortical neurones. *Nature* **278**, 850–852.

Movshon JA, Thompson ID & Tolhurst DJ (1978). Spatial and temporal contrast sensitivity of neurones in areas 17 and 18 of the cat's visual cortex. *J Physiol* **283**, 53–77.

Ohzawa I, Sclar G & Freeman RD (1985). Contrast gain-control in the cats visual-system. *J Neurophysiol* **54**, 651–667.

Orban GA (1985). Velocity tuned cortical cells and human velocity discrimination. In *Brain Mechanisms and Spatial Vision*, ed. Ingle DJ, Jeannerod M & Lee DN, pp. 371–388. Martinus Mijhof, Dordrecht.

Pennefather P, Lancaster B, Adams PR & Nicoll RA (1985). Two distinct Ca-dependent K currents in bullfrog sympathetic ganglion cells. *Proc Natl Acad Sci U S A* **82**, 3040–3044.

Price NS, Crowder NA, Hietanen MA & Ibbotson MR (2006). Neurons in V1, V2, and PMLS of cat cortex are speed tuned but not acceleration tuned: the influence of motion adaptation. *J Neurophysiol* **95**, 660–673.

Priebe NJ, Lisberger SG & Movshon JA (2006). Tuning for spatiotemporal frequency and speed in directionally selective neurons of the macaque striate cortex. *J Neurosci* **26**, 2941–2950.

Rushton WA (1965). Visual adaptation. *Proc R Soc Lond B Biol Sci* **162**, 20–46.

Sah P (1996). Ca^{2+} activated K^+ currents in neurons: types, physiological roles and modulation. *Trends Neurosci* **19**, 150–154.

Sanchez-Vives MV, Nowak LG & McCormick DA (2000a). Membrane mechanisms underlying contrast adaptation in area 17 *in vivo*. *J Neurosci* **20**, 4267–4285.

Sanchez-Vives MV, Nowak LG & McCormick DA (2000b). Cellular mechanisms of long lasting adaptation in visual cortical neurons *in vitro*. *J Neurosci* **20**, 4286–4299.

Saul AB & Cynader MS (1989a). Adaptation in single units in visual cortex: the tuning of motion aftereffects in the spatial domain. *Vis Neurosci* **2**, 593–607.

Saul AB & Cynader MS (1989b). Adaptation in single units in visual cortex: the tuning of motion aftereffects in the temporal domain. *Vis Neurosci* **2**, 609–620.

Schwindt PC, Spain WJ & Crill WE (1989). Long-lasting reduction of excitability by a sodium-dependent potassium current in cat neocortex neurons. *J Neurophysiol* **61**, 233–244.

Schwindt PC, Spain WJ & Crill WE (1992). Calcium-dependent potassium currents in neurons in cat sensorimotor cortex. *J Neurophysiol* **67**, 216–226.

Schwindt PC, Spain WJ, Foehring RC, Stafstrom CE, Chubb MC & Crill WE (1988). Multiple potassium conductances and their functions in neurons from cat sensorimotor cortex in vitro. *J Neurophysiol* **59**, 424–449.

Shou T, Li X, Zhou Y & Hu B (1996). Adaptation of visually evoked responses of relay cells in the dorsal lateral geniculate nucleus of the cat following prolonged exposure to drifting gratings. *Vis Neurosci* **13**, 605–613.

Skottun BC, De Valois RL, Grosof DH, Movshon JA, Albrecht DG & Bonds AB (1991). Classifying simple and complex cells on the basis of response modulation. *Vis Res* **31**, 1079–1086.

Solomon SG, Peirce JW, Dhruv NT & Lennie P (2004). Profound contrast adaptation early in the visual pathway. *Neuron* **42**, 155–162.

Stone J & Dreher B (1973). Projection of X- and Y-cells of the cat's lateral geniculate nucleus to areas 17 and 18 of visual cortex. *J Neurophysiol* **40**, 1051–1065.

Thompson P (1981). Velocity after-effects: the effects of adaptation to moving stimuli on the perception of subsequently seen moving stimuli. *Vis Res* **21**, 337–345.

Vidyasagar TR (1990). Pattern adaptation in cat visual cortex is a co-operative phenomenon. *Neuroscience* **36**, 175–179.

Wainwright M, Schwartz O & Simoncelli EP (2002). Natural image statistics and divisive normalization: modeling nonlinearities and adaptation in cortical neurons. In *Probabilistic Models of the Brain: Perception and Neural Function*, ed. Rao R, Olshausen B & Lewicki M, pp. 203–222. MIT Press, Cambridge, MA, USA.

Acknowledgements